catalysts

MDPI

Article

Alternating Ring-Opening Metathesis Polymerization Promoted by Ruthenium Catalysts Bearing Unsymmetrical NHC Ligands

Rubina Troiano, Chiara Costabile and Fabia Grisi *

Dipartimento di Chimica e Biologia "Adolfo Zambelli", University of Salerno, Via Giovanni Paolo II, 132, 84084 Fisciano, SA, Italy
* Correspondence: fgrisi@unisa.it; Tel.: +39-089-969557

Abstract: In this paper, Grubbs- and Hoveyda–Grubbs-type olefin metathesis catalysts featuring *N*-cyclopentyl/*N*'-mesityl backbone-substituted *N*-heterocyclic carbene (NHC) ligands were synthesized. Their propensity to promote the alternating ring-opening metathesis copolymerization (ROMP) of norbornene (NBE) with cyclooctene (COE) or cyclopentene (CPE) was evaluated and compared to that shown by analogous *N*-cyclohexyl complexes. High degrees of chemoselectivity were achieved in both copolymerizations. The presence of the *N*-cyclopentyl substituent allowed for the achievement of up to 98% and 97% of alternating diads for NBE-COE and NBE-CPE copolymers, respectively, at low comonomer ratios. Density functional theory (DFT) studies showed that both the sterical and electronic effects of NHC ligands influence catalyst selectivity.

Keywords: NHC; ruthenium complexes; ROMP; alternating copolymers; cycloolefins; DFT studies

check for updates

Citation: Troiano, R.; Costabile, C.; Grisi, F. Alternating Ring-Opening Metathesis Polymerization Promoted by Ruthenium Catalysts Bearing Unsymmetrical NHC Ligands. *Catalysts* **2023**, *13*, 34. https://doi.org/10.3390/catal13010034

Academic Editor: Shaofeng Liu

Received: 16 November 2022
Revised: 17 December 2022
Accepted: 21 December 2022
Published: 24 December 2022

1. Introduction

Since their introduction by Arduengo in 1991 [1], N-heterocyclic carbenes (NHCs) have gained increasing attention, becoming one of the most important classes of ligands in transition metal coordination chemistry [2–4]. Their strong σ-donating and adaptable π-accepting abilities make them suitable for providing stable metal–ligand frameworks with several transition metals [5–7]. The great success of NHCs is also related to the easy tunability of their steric properties, which has led to the synthesis of a plethora of different NHC architectures [8]. Accordingly, an enormous number of NHC–transition metal complexes for various catalytic applications have been reported to date [9–20].

Among them, NHC–ruthenium alkylidene complexes have been extensively studied as olefin metathesis catalysts [21,22]. These complexes have become ever more popular for their distinctive features, such as their robustness toward air and moisture, outstanding tolerance to functional groups, good thermal stability, ease of handling and high selectivity [21–24].

Many research efforts have been devoted to further enhancing the catalytic performances of this class of complexes. A successful strategy to directly influence catalyst stability, activity and selectivity involves the manipulation of the steric and electronic properties of the NHC ligand by changing substituents on the nitrogen atoms and/or the backbone of the NHC ring [25,26].

In particular, unsymmetrical substitution on the nitrogen atoms has led to the development of efficient catalysts for several specific metathesis transformations where symmetrically substituted NHC complexes fail or are scarcely efficient [26–30]. An example is the challenging synthesis of alternating copolymers via ring-opening polymerization (ROMP) of two cyclic olefins with the same olefinic double-bond polarity, such as norbornene (NBE) with cyclooctene (COE) or cyclopentene (CPE) [29,31–36]. Exceptional levels of alternation for NBE-COE (97% of alternating diads) and NBE-CPE copolymers (91% of alternating

diads) were achieved in the presence of ruthenium catalysts featuring unsymmetrically *N*,*N*′-substituted NHC (uNHC) introduced by Blechert and Buchmeiser. In both cases, the control over alternating copolymerization was facilitated by using high comonomer ratios (NBE:COE 1:50 and NBE:CPE 1:7). The selectivity in the copolymerization was correlated with the steric interaction between the 2-phenylethyl group on the nitrogen and the growing polymer chain [37–39]. The same content of alternating units (97%) in NBE-COE copolymers was obtained by Togni, who employed ruthenium complexes supported by uNHC ligands with an *N*-trifluoromethyl group. Moreover, a large excess of the less reactive monomer (COE) was required [40]. Alternating copolymers of NBE with COE, containing up to 98% of alternating diads, were synthesized at a lower NBE:COE ratio (1:10) by Plenio, using unsymmetrical *N*-alkyl,*N*′-pentiptycenyl NHC ruthenium catalysts. The better control of chemoselectivity seems to be related to the high level of dissymmetry created around the metal by the highly steric encumbered pentiptycenyl group. However, these catalysts are prepared by using a multi-step synthesis, and the obtained alternating copolymers have a high dispersity value and a low molecular weight [41] (Figure 1).

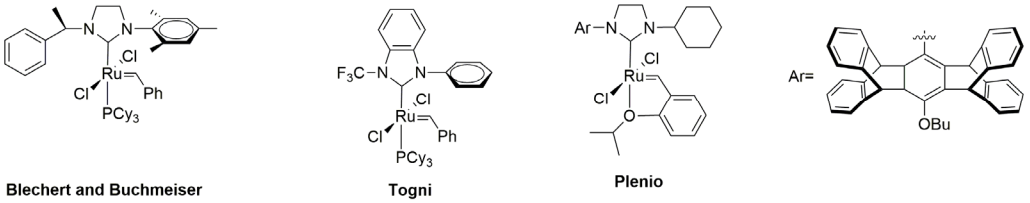

Figure 1. Grubbs- and Hoveyda–Grubbs-type catalysts with uNHCs for alternating ROMP copolymerization.

Over the last few years, we have reported on easily accessible ruthenium catalysts bearing uNHCs with *anti* and *syn* phenyl groups on the backbone [42,43]. Among them, complex **1,** possessing a *syn* backbone-substituted *N*-cyclohexyl, *N*′-mesityl NHC ligand (Figure 2), was found to be able to produce copolymers of NBE with COE or CPE with a high chemoselectivity (up to 98% or 95% of alternating diads, respectively) at low comonomer ratios (NBE:COE 1:10 and NBE:CPE 1:6), emerging as the most selective catalyst for these ROMP copolymerizations to date [44]. To further improve selectivity, we considered increasing the steric differences between the *N*-cycloalkyl and *N*′-aryl substituents of the NHC ligand, replacing the cyclohexyl group with a smaller, less flexible cyclopentyl group. Indeed, it is well-known that even a subtle change in the NHC ligand architecture can influence catalyst efficiency [25,26,30,44]. Therefore, in this study, we describe two new complexes, bearing uNHCs with *N*-cyclopentyl, *N*′-mesityl substituents and *syn* phenyl groups on the backbone (**2** and **4**, Figure 2), which are suitable for the synthesis of highly alternating NBE-COE and NBE-CPE copolymers. Their catalytic behavior is also compared with that of analogous *N*-cyclohexyl complexes **1** and **3** (Figure 2). DFT investigations are performed in order to rationalize the experimental findings.

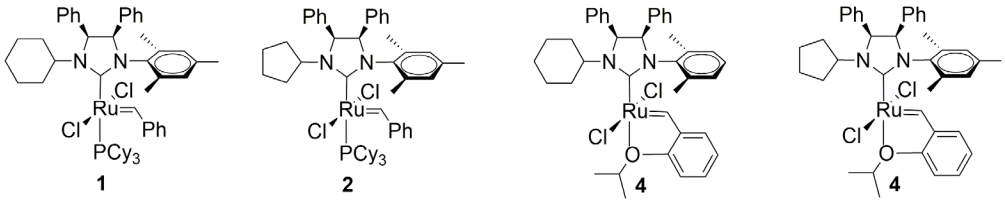

Figure 2. Ruthenium catalysts bearing *N*-cycloalkyl, *N*′-mesityl NHC ligands used in this study.

2. Results and Discussion

2.1. Synthesis of Complexes

Ruthenium complexes **1** and **3** were prepared as previously described [44,45]. The synthesis of novel complexes **2** and **4** was easily accomplished in four synthetic steps,

as depicted in Scheme 1. Diamine **A** was achieved with a yield of 69% from commercial *meso*-1,2-diphenylethylenediamine via a Pd-catalyzed cross-coupling reaction with 2-bromomesytilene. The reductive amination of cyclopentanone with **A** in the presence of sodium borohydride led to unsymmetrically substituted diamine **B** (64% yield). The cyclization of this compound with triethyl orthoformate in the presence of ammonium tetrafluoroborate furnished NHC ligand precursor **C** with a high yield (79%). The product was characterized using NMR spectroscopy and mass spectrometry (ESI-MS). The ^{1}H and ^{13}C NMR spectra of **C** showed the diagnostic resonances for the proton and for the carbon of the precarbenic position of the imidazolium salt at 8.50 ppm (NC*H*N) and 157.9 ppm (NCHN), respectively. NHC proligand **C** was deprotonated in situ with potassium *tert*-amylate and then reacted with $RuCl_2$(=CHPh)$(PCy_3)_2$ (**GI**) or $RuCl_2$(=CH-*o*-*i*PrO-Ph)(PCy_3) (**HGI**) to produce the desired complexes **2** and **4** as air- and moisture-stable solids (26% and 43%, respectively). Both complexes were characterized using NMR spectroscopy and an ESI-FT-ICR analysis (see SI). The formation of the complexes was indicated by the disappearance of the characteristic carbocationic proton of **C** in the ^{1}H NMR spectra of both **2** and **4**, along with the appearance of diagnostic peaks for the benzylidene protons at 19.68 ppm and 16.53 ppm for **2** and **4**, respectively. Consistently, the benzylidene carbon of **2** (Ru=CHPh) was observed at 297.3 ppm, whereas the benzylidene carbon of **4** (Ru=C*H*-*o*-*i*PrO-Ph) was observed at 293.1 ppm. The NHC coordination with ruthenium was also confirmed by the ^{13}C NMR signals for the carbenic carbon (*i*NCN) at 222.2 ppm for the phosphine-containing complex **2** and at 212.0 ppm for the phosphine-free complex **4**.

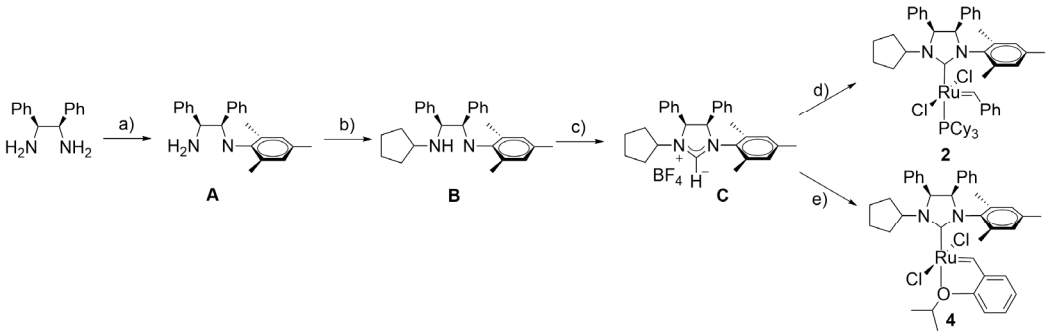

Scheme 1. Synthesis of novel uNHC ruthenium complexes **2** and **4**.

The ^{1}H and ^{31}P NMR solution spectra of **2**, recorded in C_6D_6 at room temperature, revealed the presence of only one rotational isomer corresponding to the one with the benzylidene unit located underneath the mesityl group (*anti* rotamer), as deduced from the 2D ^{1}H NMR NOESY experiments. Analogously, the solution-state structure of complex **4**, determined in the NMR studies, revealed the presence of only a single isomer, identified as the *anti* rotamer.

2.2. Alternating ROMP of Norbornene and Cyclooctene

Ruthenium complexes **1**-**4** were first compared in the ROMP copolymerization of NBE with COE (Scheme 2).

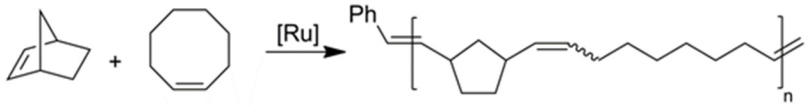

Scheme 2. Alternating ROMP of NBE and COE (ring-opening metathesis copolymerization of norbornene with cyclooctene.

The ROMP reactions were carried out under nitrogen in CH_2Cl_2, at 30 °C, employing different comonomer ratios. The results are summarized in Table 1 and Figure 3 (only for a

visual aid). In all the experiments, the immediate formation of a highly viscous solution was observed upon the addition of the catalyst. After two minutes, the polymerizations were terminated with ethyl vinyl ether, and the polymers precipitated into methanol.

Table 1. ROMP copolymerization of NBE and COE in the presence of catalysts **1**–**4**.

Entry [1]	Catalyst	NBE/COE	Poly(NBE) [%] [2,3]	Poly(COE) [%] [2,3]	Alternating Diads [%] [3]	M_n [4] (g/mol)	$Đ$ [4]	Yield (mg)
1 [5]	1	1:1	26	<1	74 (62)	9.2×10^5	1.86	167
2 [5]	1	1:4	13	<1	87 (63)	4.2×10^5	2.07	220
3 [5]	1	1:8	5	1	94 (63)	6.6×10^5	1.93	235
4 [5]	1	1:10	1	1	98 (63)	8.0×10^5	1.84	244
5	2	1:1	28	-	72 (61)	2.3×10^5	1.92	161
6	2	1:4	9	-	90 (60)	3.6×10^5	1.90	200
7	2	1:8	2	-	98 (61)	4.0×10^5	1.77	238
8	2	1:10	2	-	98 (63)	2.8×10^5	1.86	234
9	3	1:1	22	-	78 (62)	1.1×10^6	1.73	159
10	3	1:4	12	-	88 (63)	1.7×10^6	1.49	228
11	3	1:8	5	<1	95 (63)	1.1×10^6	1.79	230
12	3	1:10	2	<1	98 (63)	1.3×10^6	1.61	244
13	4	1:1	28	-	72 (61)	1.7×10^6	1.60	171
14	4	1:4	7	-	93 (62)	1.3×10^6	1.66	203
15	4	1:8	2	-	98 (63)	1.0×10^6	1.86	196
16	4	1:10	1	1	98 (62)	9.6×10^5	1.85	224

[1] Reaction conditions: CH_2Cl_2 (2.5 mL), catalyst (1.3 µmol), [NBE]/[cat] = 1000, temperature 30 °C, time 2 min. [2] Fractions of homopolymer sequences in the copolymer. [3] Determined using ^{13}C-NMR. The value in parenthesis is the percentage of *cis* double bonds. [4] Determined using THF size-exclusion chromatography (SEC) calibrated utilizing polystyrene standards. [5] See ref. [44].

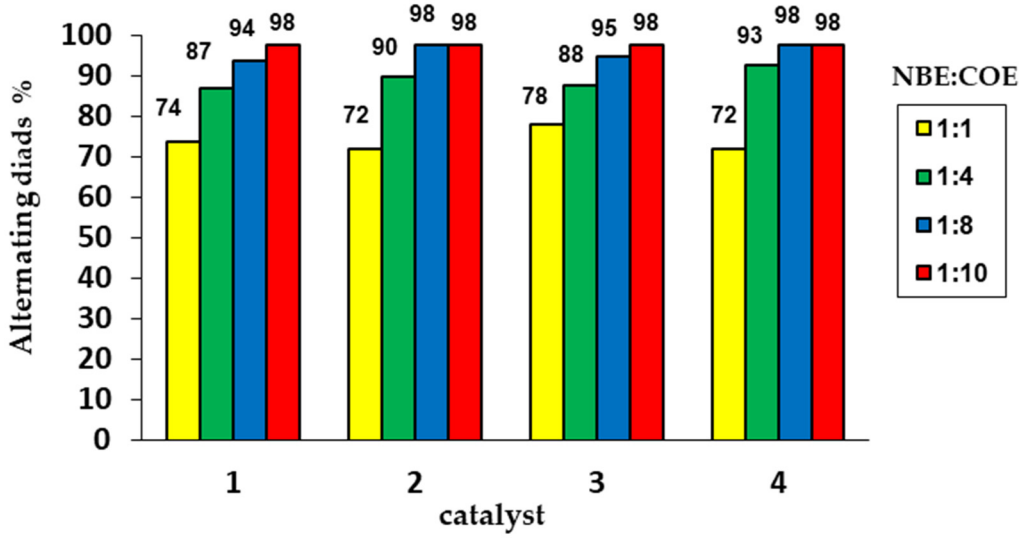

Figure 3. Content of alternating diads in the copolymers obtained at different ratios of NBE:COE (norbornene:cyclooctene).

The content of alternating diads along the copolymer chain was determined using ^{13}C NMR spectroscopy. The resonances relative to NBE-COE diads are observed in the ranges of 128.5–129.0 ppm and 134.8–135.5 ppm. The signals for NBE-NBE are found at 132.9–133.4 ppm and 133.8–134.3 ppm, while the peaks attributable to COE-COE diads are found at 130.0 and 130.5 ppm. In all the examined copolymers, only NBE-NBE diads were detected. Signals for COE-COE diads could barely be found. The representative ^{13}C NMR spectra (olefinic region) of the copolymers prepared by action **4** are shown in

Figure 4, while those relative to copolymers obtained in the presence of 2 are reported in the Supplementary Materials (Figure S8).

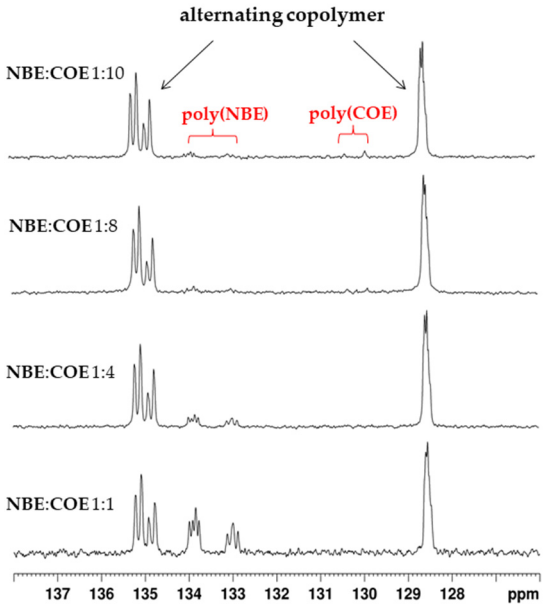

Figure 4. Olefinic region of ^{13}C NMR (150 MHz) spectra of alternating NBE-COE obtained via catalyst **4**.

The marked propensity of **1**–**4** to promote the formation of alternating sequences of NBE-COE appeared evident when an equimolar mixture of NBE and COE was employed. Indeed, a content of alternating units varying from 72 to 78% was obtained (entries 1, 5, 9 and 13 in Table 1). At the highest NBE:COE ratio (1:10), all the catalysts were able to produce an almost perfectly alternating copolymer (98% of alternating diads; see entries 4, 8, 12 and 16 and Figure 5). However, the nature of the cycloalkyl group seemed to have an effect on the chemoselectivity of the polymerization reaction. Indeed, complexes **2** and **4**, with the smaller and less flexible *N*-cyclopentyl group, showed a slightly stronger tendency to copolymerize NBE and COE in an alternating fashion with respect to the *N*-cyclohexyl catalysts **1** and **3** at an NBE:COE ratio of 1:8 (cf. entries 3 and 7 or 11 and 15). This is the lowest comonomer ratio used to date for synthesis via the ROMP of alternating NBE-COE copolymers. As a general remark, with the same *N*-cycloalkyl substituent, both the Grubbs and Hoveyda–Grubbs complexes produced copolymers with an almost identical composition. As for the stereochemistry of the carbon–carbon double bonds in the alternating copolymers, the amount of *cis* double bonds (60–63%) is consistent with that previously reported for copolymers obtained with similar catalysts.

Gel permeation chromatography (GPC) measurements of alternating copolymers (entries 4, 7,8, 12, 15 and 16) showed number-average molecular weights in the range of 230,000 < *Mn* < 1,000,000 g/mol. All these copolymers had a monomodal distribution with moderately narrow dispersities (1.61 < *Đ* < 1.86). The experimental M_n values were higher than the theoretical ones (e.g., *Mn* = 184,000 g/mol for copolymer of entry 8 calculated by considering that the conversion of NBE (and COE) was 90%), suggesting that incomplete catalyst initiation or slow initiation over propagation occurred. When Hoveyda–Grubbs-type catalysts **3** and **4** were employed, M_n values higher than those observed in the presence of Grubbs complexes **1** and **2** were obtained. This finding could be related to the different initiation mechanism involved in the two families of catalysts [46–52].

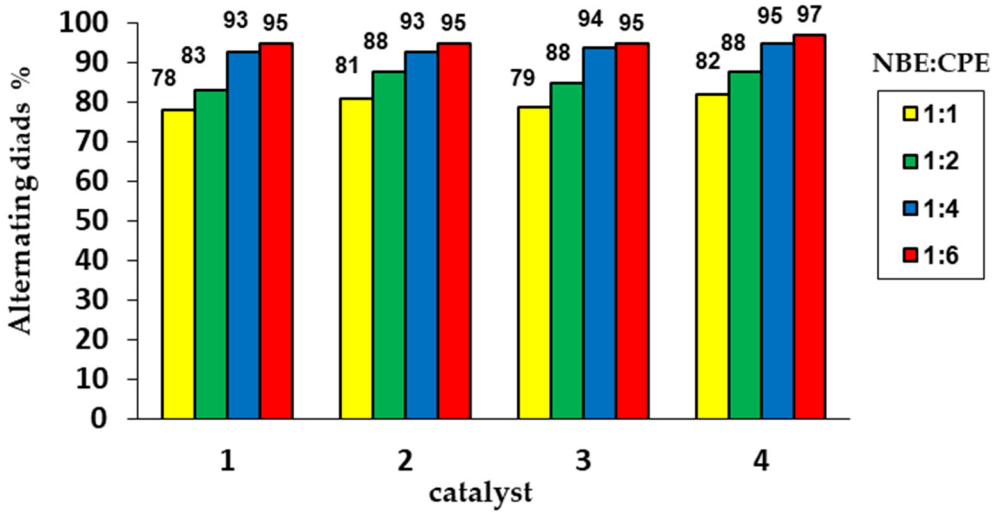

Figure 5. Content of alternating diads in the copolymers obtained at different ratios of NBE:CPE (norbornene:cyclopentene).

Differential scanning calorimetric (DCS) measurements of the alternating copolymers showed only the glass transition temperature (*T*g) for each polymer sample. The *T*g values were observed in the range from −46.08 to −52.70 °C (Figures S10, S12, S14, S16 in the Supplemetary Materials), in line with the *T*g values reported for similar copolymers [38].

2.3. Alternating ROMP of Norbornene and Cyclopentene

Ruthenium complexes **1–4** were then investigated in the alternating copolymerization of NBE with CPE (Scheme 3), under the same experimental conditions used for the NBE-COE copolymerization experiments. A prolonged reaction time (15 min) was used, as CPE has a lower propensity than COE to undergo ROMP [53]. The results are displayed in Table 2 and Figure 5 (only for a visual aid).

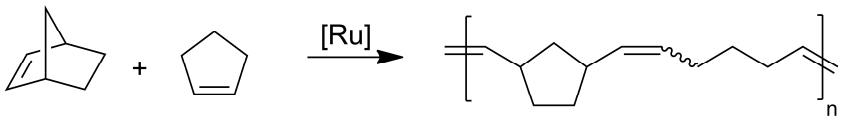

Scheme 3. Alternating ROMP of NBE and CPE (ring-opening metathesis copolymerization of norbornene with cyclopentene).

The amount of alternating diads in the obtained copolymers was determined using ^{13}C-NMR spectroscopy. The resonances relative to NBE-CPE diads are found in the range of 128.1–128.7 ppm and 135.0–135.8 ppm. The signals for NBE-NBE are observed at 132.9–133.4 ppm and 133.8–134.3 ppm, while the peaks attributable to CPE-CPE diads are observed at 130.0 and 130.5 ppm. Besides NBE-NBE homosequences, signals for CPE-CPE diads are detectable in some ^{13}C-NMR spectra of the copolymers.

As an example, the olefinic region of the ^{13}C-NMR spectra for the copolymers obtained with **4** is shown in Figure 6. The ^{13}C NMR spectra of copolymers obtained with 2 are shown in the Supplementary Materials (Figure S9). As previously observed, all the catalysts were able to promote the copolymerization of NBE and CPE in an alternating fashion. Elevated levels of alternation (78–82%) were achieved, even at a 1:1 comonomer ratio (Figure 5). Moreover, by using an NBE:CPE ratio of only 1:4, copolymers containing 93–95% of alternating diads were obtained. In the presence of *N*-cyclopentyl catalyst **4**, at the highest comonomer ratio (1:6), a nearly perfectly alternating NBE-CPE copolymer was formed (97% of alternating units; entry 16 in Table 2). This percentage of alternating units is the highest value found to date for NBE-CPE copolymers.

Table 2. ROMP copolymerization of NBE and CPE in the presence of catalysts **1**–**4**.

Entry [1]	Catalyst	NBE/CPE	Poly(NBE) [%] [2,3]	Poly(CPE) [%] [2,3]	Alternating Diads [%] [3]	M_n [4] (g/mol)	$Đ$ [4]	Yield (mg)
1 [5]	**1**	1:1	22	<1	78	8.7×10^4	1.59	163
2 [5]	**1**	1:2	17	<1	83	7.1×10^4	1.63	115
3 [5]	**1**	1:4	7	<1	93	1.0×10^5	1.78	135
4 [5]	**1**	1:6	5	<1	95	1.1×10^5	1.87	165
5	**2**	1:1	19	-	81	1.8×10^5	2.10	163
6	**2**	1:2	12	<1	88	1.6×10^5	1.95	172
7	**2**	1:4	6	1	93	1.5×10^5	2.18	186
8	**2**	1:6	3	2	95	1.5×10^5	2.28	200
9	**3**	1:1	21	-	79	3.1×10^5	1.98	157
10	**3**	1:2	15	-	85	1.8×10^5	1.96	165
11	**3**	1:4	6	<1	94	2.0×10^5	2.01	179
12	**3**	1:6	4	1	95	1.3×10^5	1.70	171
13	**4**	1:1	18	-	82	3.2×10^5	1.64	151
14	**4**	1:2	12	-	88	2.0×10^5	1.85	176
15	**4**	1:4	5	-	95	3.3×10^5	1.97	168
16	**4**	1:6	3	<1	97	2.1×10^5	1.95	172

[1] Reaction conditions: CH_2Cl_2 (2.5 mL), catalyst (1.3 μmol), [NBE]/[cat] = 1000, temperature 30 °C, time 15 min. [2] Fractions of homopolymer sequences in the copolymer. [3] Determined using ^{13}C-NMR. [4] Determined using THF size-exclusion chromatography (SEC) calibrated using polystyrene standards. [5] See Ref. [44].

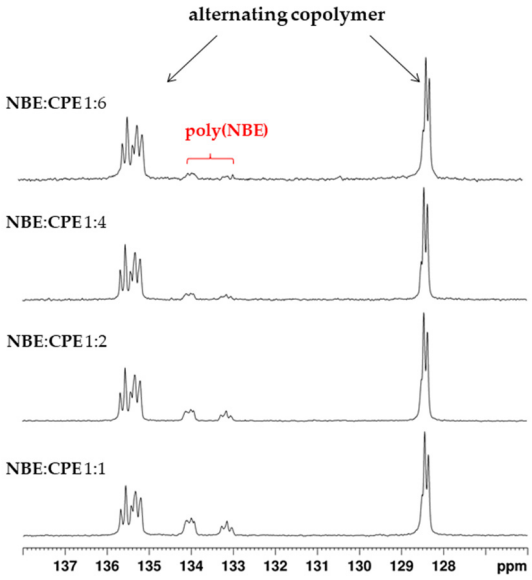

Figure 6. Olefinic region of ^{13}C-NMR (150 MHz) spectra of alternating NBE-CPE (norbornene cyclopentene) copolymers obtained via catalyst **4**.

The alternating copolymers (entries 4, 8, 12 and 16 in Table 2) were characterized by relatively high molecular weights (110,000 < M_n < 330,000 g/mol) and unimodal molecular weight distributions (1.87 < $Đ$ < 2.28). DSC thermograms of the alternating copolymers showed only one single Tg for each copolymer in the range of $-29.8 < T_g < -31.7$ °C (Figures S11, S13, S15, S17 in the Supplementary Materials). Again, these T_g values are comparable to those reported for previously obtained alternating NBE-CPE copolymers [37,38].

2.4. Molecular Modeling Studies

The exceptional selectivity of catalysts 1–4 toward alternating NBE-COE and NBE-CPE copolymerization, obtained even at a 1:1 comonomer ratio (72–78% of alternation

NBE-COE/78–82% of alternation NBE-CPE), encouraged us to perform molecular modeling studies to gain additional information on the catalyst structures. In more detail, we optimized the geometries of catalysts 3 and 4 via DFT calculations (see SI for computational details) and compared the minimum energy structures with those obtained via the optimization of the Buchmeiser catalyst (5a in Ref. [38], the Hoveyda–Grubbs version of the Blechert and Buchmeiser catalyst in Figure 1) (Figure 7). This catalyst showed good but not excellent selectivities in alternating copolymerization (for a 1:1 comonomer ratio, 40% of alternation NBE-COE/55% of alternation NBE-CPE), although the catalyst structure is very similar to that of 3 and 4. The minimum energy geometries and relevant parameters are reported in Figure 4. According to the computational results, complexes 3 and 4 exhibit a more pronounced proximity of the *N*-alkyl substituent to the metal with respect to the Buchmeiser catalyst. This is evidenced by the shorter Ru–C distances for *N*-alkyl carbon (~3.18 Å) and by the stronger Ru-H interactions of the *N*-alkyl group (Ru-H distance ~2.45 Å). Complexes 3 and 4 also showed a smaller C-C-C bond angle of the *N*-cycloalkyl carbon.

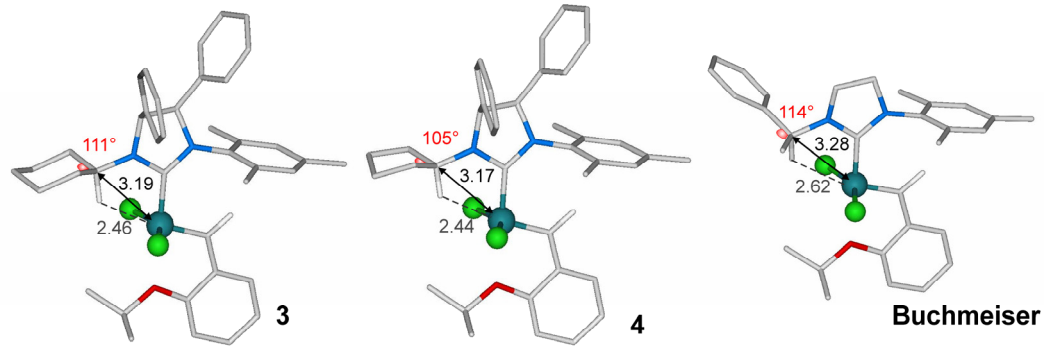

Figure 7. Minimum energy structures of catalysts 3 [45] and 4, as well as the Buchmeiser catalyst. Most hydrogens were omitted for clarity. Distances are in Å.

Quantitative information on the catalytic pocket of optimized structures has previously been obtained by modeling topographic steric maps [54,55] and by calculating the percent buried volumes (%V_{Bur}). %V_{Bur} is a parameter that quantifies the steric hindrance of ligands and is defined as the fraction of the total volume of a sphere centered on the metal occupied by a given ligand [56,57].

Topographic steric maps, shown in Figure 8, were obtained (with a program on the SambVca web server) [54,55] starting from the optimized minimum energy structures of the complexes in Figure 7. The complexes are oriented according to the structure on the top of the map. The NHC ligand is located behind the xy plane, and the iso-contour curves indicate how deeply the NHC ligands protrude out of the xy plane occupying the space around the metal. More intense green-yellow lines indicate a stronger steric pressure of the ligand in that area. For every map in Figure 8, the overall %V_{Bur} and %V_{Bur} values for each quadrant are reported.

According to the topographic steric maps, the overall %V_{Bur} is slightly higher for complexes **3** and **4** (31.8 and 31.7, respectively) with respect to the Buchmeiser catalyst (31.2). Not surprisingly, all complexes show a dissymmetry of steric hindrance, with respect to the plane perpendicular to the NHC plane, due to the unsymmetrical *N*-substitution and the presence of alkydene on one side of the catalyst (NW-SW vs. NE-SE quadrants). More interesting is the dissymmetry in the %V_{Bur} value of the NE and SE quadrants for catalysts **3** and **4**, which is flattened in the Buchmeiser catalyst. This dissymmetry is mainly due to the presence of the *syn* Ph groups on the NHC backbone of complexes **3** and **4**, as it induces a dissymmetry of the catalytic pocket with respect to the plane of the NHC.

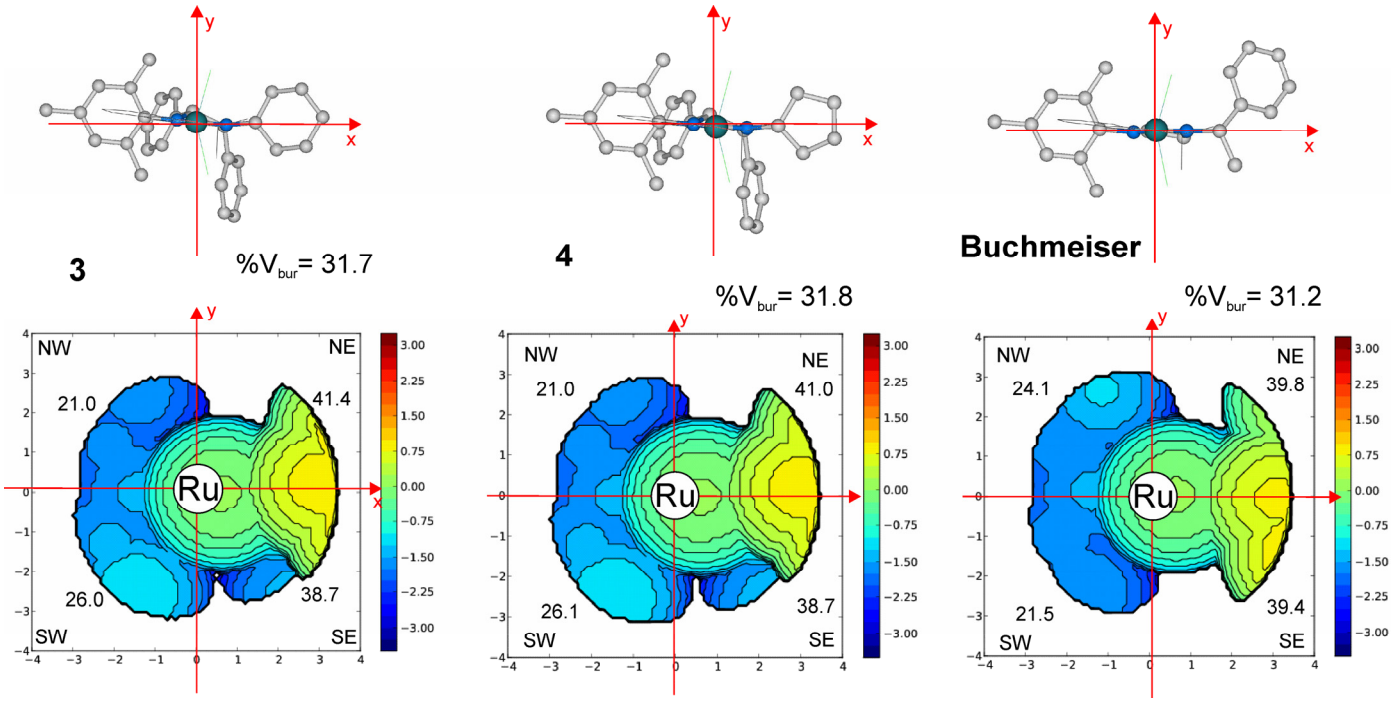

Figure 8. Topographic steric maps of 3 [45], 4 and Buchmeiser catalyst. The iso-contour curves of steric maps are in Å. The maps were constructed starting from the minimum energy structures of complexes optimized via DFT calculations. The complexes are oriented according to the structure on the top of the map. Overall %*V*Bur and %*V*Bur representative of each single quadrant are reported for each map. %*V*Bur is a parameter that quantifies the steric hindrance of ligands and is defined as the fraction of the total volume of a sphere centered on the metal occupied by a given ligand [56,57]. Quadrants in topographic steric maps are identified as NW, NE, SW and SE, according to their position on the map.

To investigate the influence of the catalytic pocket shape on alternating copolymerization, the CPE and NBE minimum energy coordination structures were located. The geometries and free coordination energies in CH_2Cl_2 (see SI for computational details) are depicted in Figure 9. For all structures, the π interaction between olefin and metal results in a stretching of the C=C double bond (for coordinated CPE, the C=C distance is 1.39 Å vs. 1.35 Å for free CPE; for coordinated NBE, the C=C distance is 1.40 Å vs. 1.35 Å for free NBE). According to the computational results, all catalysts exhibit lower coordination energies for NBE with respect to CPE. This finding is in agreement with the higher reactivity of norbornene in the copolymerization. Nevertheless, the ΔΔG of the CPE coordination is significantly lower for **3** and **4**, with respect to the Buchmeiser catalyst (see Table 3). Indeed, **3** and **4** show a coordination energy for CPE that is only 0.7 kcal/mol higher than that for NBE, whereas the energy gap is 2.0 kcal/mol for the Buchmeiser catalyst. As shown in Figure 9, comparing the NBE minimum energy coordination structures, slightly shorter NBE-Cl and NBE-alkylidene distances are observed for **3** and **4**, as a possible effect of phenyls on the NHC backbone. This suggests the presence of sterical interactions slightly penalizing NBE coordination with **3** and **4** with respect to the Buchmeiser catalyst.

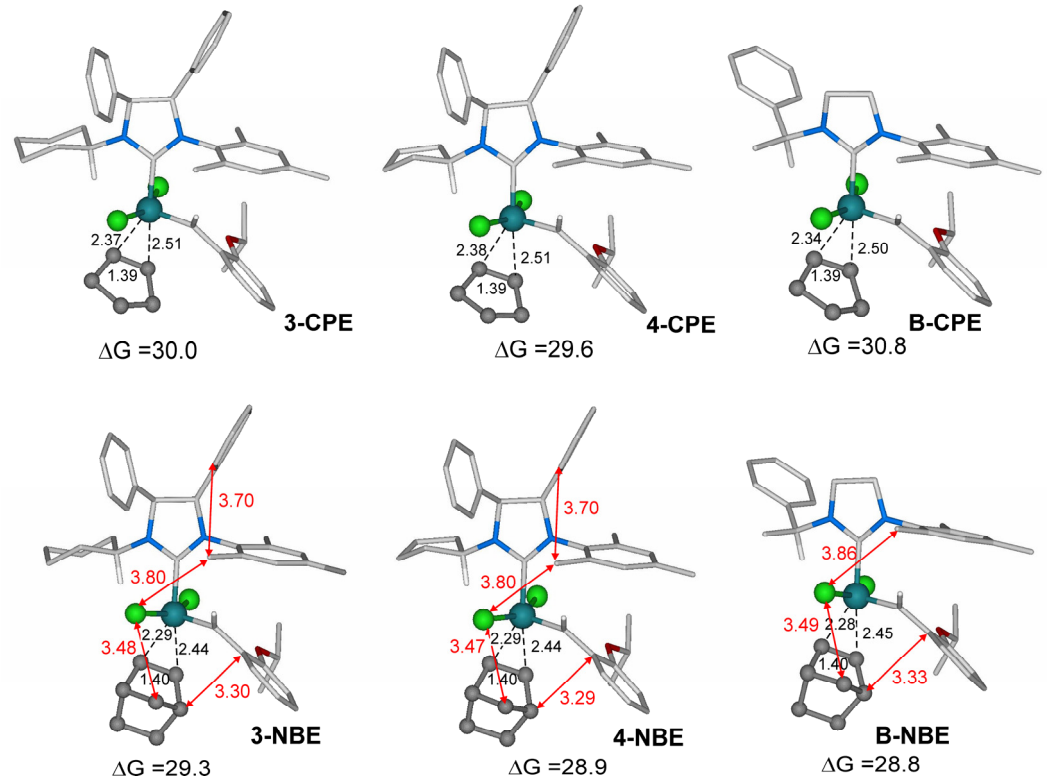

Figure 9. CPE and NBE minimum energy coordination structures for catalyst **3** (**3-CPE** and **3-NBE**), catalyst **4** (**4-CPE** and **4-NBE**) and **Buchmeiser** catalyst (**B-CPE** and **B-NBE**). Free energies of CPE and NBE coordination in CH_2Cl_2 are in kcal/mol.

Table 3. $\%V_{Bur,}$ ΔΔG monomer coordination and Ru charge of **3**, **4** and Buchmeiser catalyst.

Catalyst	$\%V_{Bur}$ [1]	ΔΔG [2]	Ru Charge [3]
3	31.7	0.7	−0.30214
4	31.8	0.7	−0.30677
Buchmeiser	31.2	2.0	−0.29546

[1] $\%V_{Bur}$ of topographic maps reported in Figure 8. [2] ΔΔG represents the energy difference between the coordination energy of CPE and the coordination energy of NBE ($\Delta\Delta G = \Delta G_{CPE} - \Delta G_{NBE}$). [3] Ru charges were obtained from NBO analysis.

Finally, to gain information on the electronic effects of the different NHC ligands on the catalyst behavior, we calculated the Ru charge for all catalysts by carrying out a natural bond orbital (NBO) analysis. As shown in Table 3, the absolute value of the negative charges of Ru decreases in the order **4** > **3** > **Buchmeiser**. The lower coordination free energy observed for the Buchmeiser catalyst for the more electron-donating NBE could partially be a consequence of the less negative Ru charge.

In summary, according to the DFT studies, **3** and **4** present higher $\%V_{Bur}$ for NHC moiety, which also entails a dissymmetrical distribution of the catalytic pocket due to the *syn* phenyls on the backbone. The coordination of NBE with CPE is more favored for the Buchmeiser catalyst with respect to **3** and **4**, which is in agreement with the lower percentage of alternating copolymers produced by this catalyst. This difference may be caused by both sterical and electronic effects.

3. Materials and Methods

3.1. General Information

All the operations of synthesis and handling involving sensitive chemicals were performed under a nitrogen atmosphere in a glovebox or by using standard Schlenk techniques.

The glassware and vials used were dried in an oven at 120 °C overnight and exposed to a vacuum–nitrogen cycle three times. Commercially available starting materials and solvents were purchased from Merck Italy (Milan, Italy). Toluene and methylene chloride were purchased from Merck, suitably dried (over sodium and lithium aluminum hydride, respectively) and distilled before use. Deuterated solvents were dried over activated 4 Å molecular sieves prior to use. Organic molecules and organometallic compounds were purified through flash column chromatography using silica gel 60 (230–400 mesh) purchased from Merck Italy (Milan, Italy) and TSI Scientific (Cambridge, Massachusetts, United States), respectively. Thin-layer chromatography (TLC) was performed using silica gel 60 aluminum foils with an F254 fluorescence indicator.

Complexes [1-cyclohexyl-3-mesityl-4,5-diphenyl-2-imidazolidinylidene](dichloro)(benzilydene)(tricyclohexylphosphine) (**1**), [1-cyclohexyl-3-mesityl-4,5-diphenyl imidazolidinylidene]dichloro(2-isopropoxyphenylmethylene)ruthenium (**3**) and N^1-mesityl-1,2-diphenylethane-1,2-diamine (**A**) were synthesized according to procedures detailed in the literature [44,45].

NMR experiments were carried out on a Bruker AM 300 (Bruker, Germany) (300 MHz for ^{1}H; 75 MHz for ^{13}C), Bruker AVANCE 400 ((Bruker, Germany) 400 MHz for ^{1}H; 100 MHz for ^{13}C; 161.97 MHz for ^{31}P) and Bruker ASCEND 600 (Bruker, Germany) (600 MHz for ^{1}H; 150 MHz for ^{13}C). Chemical shifts in the spectra were reported as follows: chemical shift (ppm), multiplicity and integration. Multiplicity was abbreviated as follows: singlet (s), doublet (d), triplet (t), multiplet (m), broad (br) and overlapped (o). ^{1}H and ^{13}C-NMR chemical shifts are listed in parts per million (ppm) downfield from tetramethyl silane (TMS) as the internal standard. ^{31}P chemical shifts are referenced using H_3PO_4 as the external standard.

An ESI-MS analysis was performed on a Waters spectrometer (Waters Corporation, Milford, Massacchussets, United States) with an electrospray source. An ESI-FT-ICR analysis of ruthenium complexes was carried on a Bruker Solarix XR spectrometer ((Bruker Daltonik GmbH, Bremen, Germany). GPC measurements were performed on a Waters 1525 binary equipped with a Waters 2414 RI detector using four Styragel columns (range 1000–1,000,000 Å) (Waters Corporation, Milford, Massacchussets, United States).

DSC measurements were carried out on a DSC Q20 apparatus, manufactured by TA Instruments Waters/TA instruments, New Castle, Delaware, United States), in flowing N_2 with a cooling and heating rate of 10°C /min.

3.2. Synthesis of N^1-Cyclopentyl-N^2-Mesityl-1,2-Diphenylethane-1,2-Diamine (B)

Diamine **A** (1 equiv.), cyclopentanone (7 equiv.) and dry methylene chloride (C = 0.1 M) were introduced into a round-bottom flask. The reaction mixture was stirred at room temperature over activated molecular sieves 4 Å for three days and then filtered. Afterward, the solvent was removed under vacuum, the crude reaction product was diluted with dry methanol (C = 0.1 M), and $NaBH_4$ (7 equiv.) was added in three portions.

The reaction mixture was stirred for 4 h, diluted with methylene chloride and extracted with water. The organic phase was dried over Na_2SO_4 and filtered, and then the solvent was removed under reduced pressure. The product was obtained as an oil, which was purified using flash column chromatography on silica gel (hexane: ethyl acetate 9:1) to produce a white solid (yield 64%).

^{1}H-NMR ($CDCl_3$, 400 MHz): δ 7.27–7.23 (o m, 3H); 7.16–7.10 (o m, 3H); 6.93–6.90 (o m, 2H); 6.83–6.81 (o m, 2H); 6.68 (br s, 2H); 4.50 (d, J = 4.8, 1H); 4.24 (d, J = 4.7, 2H); 2.89 (m, 1H); 2.15 (s, 9H); 1.70 (o m, 3H); 1.48 (o m, 3H), 1.28 (o m, 2H) (Figure S1 (top) in the Supplementary Materials).

^{13}C-NMR ($CDCl_3$, 100 MHz): δ 142.51; 141.02; 139.52; 129.66; 129.07; 128.31; 127.94; 127.87; 127.52; 127.03; 127.01; 126.90; 66.51; 65.32; 56.38; 35.60; 34.38; 32.43; 23.85; 20.45; 19.63 (Figure S1 (bottom) in the Supplementary Materials).

ESI+MS: m/z = 399.3 (MH^+).

3.3. Synthesis of 1-Cyclohexyl-3-Mesityl-4,5-Diphenyl-4,5-Dihydro-1H-Imidazol-3-Ium Tetrafluoroborate (C)

Diamine **B** (1 equiv.) and triethyl orthoformate (8 equiv.) were introduced into a round-bottom flask, equipped with a magnetic stirrer and a condenser. The mixture was stirred at room temperature for five minutes. After that, ammonium tetrafluoroborate (1.2 equiv.) was added, and the mixture was heated at 130 °C for 2 h. Subsequently, the condenser was removed to facilitate the evaporation of the ethanol produced during the reaction. A crude brownish oil was obtained, which was then washed with diethyl ether and purified using flash column chromatography on silica gel (hexane: ethyl acetate 9:1 to 1:1) to produce a white solid (yield 85%).

$^{1.}$ H-NMR ($CDCl_3$, 400 MHz): δ 8.50 (s, 1H); 7.22 (br s, 3H); 7.01 (m, 3H); 6.93 (t, J = 7.7 Hz, J = 7.6, 2H); 6.83 (br s, 1H); 6.78 (d, J = 11.6 Hz, 1H); 5.89 (dd, J = 11.8 Hz, J = 3.2 Hz, 1H); 4.13 m, 1H); 2.48 (s, 3H); 2.32 (s, 3H); 2.28 (br m, 1H); 2.14 (s 3H); 2-06-1.52 (overlapping signals, 9H) (Figure S2 (top) in the Supplementary Materials).

^{13}C-NMR ($CDCl_3$, 100 MHz): δ 157.89,139.40; 135.07; 134.36; 131.70; 130.94; 130.34; 129.81; 129.27; 129.02; 128.22; 127.51; 72.70; 68.91; 60.26; 31.47; 31.42; 22.99; 22.86; 20.90; 19.63; 19.42 (Figure S2 (bottom) in the Supplementary Materials).

ESI+MS: m/z = 409.3 [M^+(-$BF4^-$)]

3.4. Synthesis of [1-Cyclopentyl-3-Mesityl-4,5-Diphenyl-2-Imidazolidinylidene](Dichloro) (Benzilydene)(Tricyclohexylphosphine)Ruthenium (2)

In a glovebox, under a nitrogen atmosphere, a Schlenk tube was charged with tetrafluoroborate salt **C** (1 equiv.) and dry toluene (C = 0.026 M). Potassium *tert*-amylate (1 equiv.) was then added to the resulting suspension, and the reaction mixture was stirred for five minutes at room temperature. After that, **GI** (1 equiv.) was added. The flask was removed from the glovebox and kept under stirring at room temperature for 0.5 h. The crude reaction mixture was purified using flash column chromatography on silica gel (hexane: diethyl ether 9:1 to 1:1) to produce the desired complex as a pink brownish solid (yield 26%).

^{1}H-NMR (C_6D_6, 400 MHz): δ 19.68 (br s, 1H) (Ru = C*H*Ph); 9.01 (br s, 1H); 7.50 (br s, 1H); 7.14 (overlapping signals, 4H); 7.06 (m, 4H); 6.88 (o m, 3H); 6.59 (m, 2H); 6.48 (br m, 2H); 6.03 (overlapping signals, 3H); 5.79 (m, 1H); 5.03, d, J = 9,1 Hz, 1H); 3.27 (m, 1H); 2.69–1.88 (overlapping signals, 41H) (Figure S3 (top) in the Supplementary Materials).

^{13}C-NMR (C_6D_6, 150 MHz):) 297.26 (br s, Ru = *C*HPh); 222.22 (*i*NCN) ($^2J_{C-P}$ = 77.90 Hz); 151.82; 138.33; 136.86; 136.74; 136.04; 133.17; 133.15; 129.63; 127.49; 75.42; 64.98; 64.02; 32.54; 32.45; 30.92; 29.94; 28.25; 26.94; 24.68; 23.76; 21.03; 20.72 (Figure S3 (bottom) in the Supplementary Materials).

^{31}P-NMR (C_6D_6, 161.97 MHz): δ 29.32 (Figure S4 in the Supplementary Materials).

ESI-FT-ICR (**2**-Cl): m/z calcd 915.4093, found 915.4093 (Figure S6 in the Supplementary Materials).

3.5. Synthesis of 1-Cyclopentyl-3-Mesityl-4,5-Diphenyl-2-Imidazolidinylidene](Dichloro) (Benzily-Dene)(2-Isopropoxyphenylmethylene)Ruthenium (4)

In a glovebox, under a nitrogen atmosphere, a Schlenk tube was charged with tetrafluoroborate salt **C** (1 equiv.) and dry toluene (C = 0.026 M). Potassium *tert*-amylate (1 equiv.) was then added to the resulting suspension, and the reaction mixture was stirred for five minutes at room temperature. After that, **HGI** (1 equiv.) was added, and the flask was removed from the glovebox and kept under stirring at room temperature for 0.5 h. The crude reaction mixture was purified using flash column chromatography on silica gel (hexane: diethyl ether 9:1 to 1:1) to produce the desired complex as a green solid (yield 43%).

^{1}H-NMR (C_6D_6, 600 MHz): δ 16.53 (s, 1H) (Ru=C*H*-o-iPrOPh); 8.80 (br s, 1H); 7.39–7.06 (o m, 7H); 6.67–6.56 (o m; 7H); 6.47 (d, 1H, J = 7.7); 6.14 (m, 1H), 6.03 (d, 1H, J = 8.2 Hz), 4.98 (d, 1H, J = 8.3 Hz); 4.69 (m, 1H); 3.14 (br m, 1H), 2.61–2.1 (overlapping signals, 7H); 1.95 (s, 3H); 1.81–1.75 (overlapping signals, 8H), 1.62 (br m, 2H); 1.62 (br m, 3H), 1.46–1.31 overlapping signals, 2H) (Figure S5 (top) in the Supplementary Materials).

^{13}C-NMR (CD_2Cl_2, 75MHz): 293.13 (Ru=CH-o-iPrO-Ph); 211.99 (*i*NCN); 152.26; 144.22; 139.49; 138.19; 137.63; 136.60; 136.00; 132.48; 130.12; 129.69; 129.39; 129.16; 128.16; 128.02; 127.74; 127.48; 122.57; 122.43; 112.94; 75.02; 65.57; 64.35; 30.90; 30.43; 23.42; 22.35; 21.72; 21.63; 20.67; 19.66; 19.58 (Figure S5 (bottom) in the Supplementary Materials).

ESI-FT-ICR (**4**-Cl): *m*/*z* calcd 693.2210, found 693.2188 (Figure S7 in the Supplementary Materials).

3.6. General Polymerization Procedure

Norborn-2-ene (1.3 mmol, 1 equiv.) and an appropriate amount of *cis*-cyclooctene or cyclopentene were dissolved in methylene chloride and warmed to 30 °C. A methylene chloride solution of catalysts (1.3 μmol) was then injected. The polymerization was quenched by adding ethyl vinyl ether, and the polymer formed was coagulated in methanol, recovered via filtration and dried under vacuum.

4. Conclusions

In this study, new Grubbs- and Hoveyda–Grubbs-type complexes possessing an unsymmetrical *N*-cyclopentyl, *N*′-mesityl NHC ligand, with *syn* phenyl groups on the backbone, were synthesized. Their catalytic behavior was investigated in the alternating ROMP of NBE with COE or CPE and compared to that of corresponding *N*-cyclohexyl complexes. All the complexes were found to be able to produce copolymers with exceptional levels of alternation, and no difference in chemoselectivity between the two families of catalysts was observed. As for the *N*-cycloalkyl substituent, the replacement of the cyclohexyl group with the less sterically encumbered and less flexible cyclopentyl group led to an almost perfectly alternating polymer, NBE-COE, at the lowest comonomer ratio (1:8) reported to date. Moreover, *N*-cyclopentyl catalyst **4** was identified as the most selective in the alternating copolymerization of NBE-CPE, producing 97% of alternating units at a comonomer ratio of 1:6. Moreover, in this case, to the best of our knowledge, this represents the highest value achieved to date. Notably, all the alternating copolymers obtained possessed relatively high molecular weights and moderately narrow dispersities.

According to the DFT studies, **3** and **4** presented a dissymmetrical shape of the catalytic pocket due to the *syn* phenyls on the backbone. The coordination of NBE was only slightly favored with respect to CPE, which is in agreement with the high percentage of alternating copolymers produced by these catalysts. A comparison with similar unsymmetrical NHC-Ru catalysts indicated that both sterical and electronic effects of the NHC ligands in **3** and **4** may be involved in determining the selectivity in copolymerization.

A deeper investigation into possible combinations of *N*-alkyl and *N*′-aryl substituents of different bulkiness to further improve chemoselectivity in the alternating ROMP copolymerization is currently underway.

Supplementary Materials: The following supporting information can be downloaded at: https://www.mdpi.com/article/10.3390/catal13010034/s1, Figures S1–S5: NMR spectra of **B**, **C**, **2** and **4**; Figures S6 and S7: ESI-FT-ICR spectra of **2** and **4**; Figures S8 and S9: olefinic regions of ^{13}C NMR spectra of copolymers obtained via **2**; Figures S10–S17: DSC thermograms of alternating copolymers; computational details. References [58–67] are cited in the Supplementary Materials

Author Contributions: Investigation and validation, R.T.; conceptualization, data curation and writing—original draft preparation, C.C.; conceptualization, resources, formal analysis, writing—original draft, writing—review and editing, supervision and project administration, F.G. All authors have read and agreed to the published version of the manuscript.

Funding: This research received no external funding.

Data Availability Statement: Not applicable.

Acknowledgments: Financial support was provided by the University of Salerno (FARB) and by the INNOLUBE project 2017–2020. We thank Patrizia Oliva (University of Salerno), Mariagrazia Napoli (University of Salerno) and Patrizia Iannece (University of Salerno) for technical assistance. F.G. thanks Simone Pappalardo for some experimental work.

Conflicts of Interest: The authors declare no conflict of interest.

References

1. Arduengo, A.J.; Harlow, R.L.; Kline, M. A Stable Crystalline Carbene. *J. Am. Chem. Soc.* **1991**, *113*, 361–363. [CrossRef]
2. Nolan, S.P. (Ed.) *N-Heterocyclic Carbenes in Synthesis*, 1st ed.; WileyWILEY-VCH Verlag GmbH & Co. KGaA: Weinheim, Germany, 2006; ISBN 978-3-527-31400-3.
3. Glorius, F. *N-Heterocyclic Carbenes in Transition Metal Catalysis*; Topics in Organometallic Chemistry; Springer Berlin Heidelberg: Berlin/Heidelberg, Germany, 2007; Volume 21, ISBN 978-3-540-36929-5.
4. Hopkinson, M.N.; Richter, C.; Schedler, M.; Glorius, F. An Overview of N-Heterocyclic Carbenes. *Nature* **2014**, *510*, 485–496. [CrossRef] [PubMed]
5. Nelson, D.J.; Nolan, S.P. Quantifying and Understanding the Electronic Properties of N-Heterocyclic Carbenes. *Chem. Soc. Rev.* **2013**, *42*, 6723. [CrossRef] [PubMed]
6. Dröge, T.; Glorius, F. The Measure of All Rings-N-Heterocyclic Carbenes. *Angew. Chem. Int. Ed.* **2010**, *49*, 6940–6952. [CrossRef] [PubMed]
7. Jacobsen, H.; Correa, A.; Poater, A.; Costabile, C.; Cavallo, L. Understanding the M-(NHC) (NHC = N-Heterocyclic Carbene) Bond" Coordin. *Chem. Rev.* **2009**, *253*, 687–703. [CrossRef]
8. Nolan, S.P. *N-Heterocyclic Carbenes: Effective Tools for Organometallic Synthesis*; John Wiley & Sons: Hoboken, NJ, USA, 2014; ISBN 978-3-527-67124-3.
9. Lin, J.C.Y.; Huang, R.T.W.; Lee, C.S.; Bhattacharyya, A.; Hwang, W.S.; Lin, I.J.B. Coinage Metal-*N*-Heterocyclic Carbene Complexes. *Chem. Rev.* **2009**, *109*, 3561–3598. [CrossRef]
10. Visbal, R.; Gimeno, M.C. N-Heterocyclic Carbene Metal Complexes: Photoluminescence and Applications. *Chem. Soc. Rev.* **2014**, *43*, 3551–3574. [CrossRef]
11. Zhang, D.; Zi, G. N-Heterocyclic Carbene (NHC) Complexes of Group 4 Transition Metals. *Chem. Soc. Rev.* **2015**, *44*, 1898–1921. [CrossRef]
12. Bellemin-Laponnaz, S.; Dagorne, S. Group 1 and 2 and Early Transition Metal Complexes Bearing N-Heterocyclic Carbene Ligands: Coordination Chemistry, Reactivity, and Applications. *Chem. Rev.* **2014**, *114*, 8747–8774. [CrossRef]
13. Lee, J.; Hahm, H.; Kwak, J.; Kim, M. New Aspects of Recently Developed Rhodium(N-Heterocyclic Carbene)-Catalyzed Organic Transformations. *Adv. Synth. Catal.* **2019**, *361*, 1479–1499. [CrossRef]
14. Peris, E. Smart N-Heterocyclic Carbene Ligands in Catalysis. *Chem. Rev.* **2018**, *118*, 9988–10031. [CrossRef] [PubMed]
15. Zhao, Q.; Meng, G.; Nolan, S.P.; Szostak, M. N-Heterocyclic Carbene Complexes in C–H Activation Reactions. *Chem. Rev.* **2020**, *120*, 1981–2048. [CrossRef] [PubMed]
16. Pan, Y.; Jiang, X.; So, Y.-M.; To, C.T.; He, G. Recent Advances in Rare Earth Complexes Containing N-Heterocyclic Carbenes: Synthesis, Reactivity, and Applications in Polymerization. *Catalysts* **2020**, *10*, 71. [CrossRef]
17. César, V.; Bellemin-Laponnaz, S.; Gade, L.H. Chiral N-Heterocyclic Carbenes as Stereodirecting Ligands in Asymmetric Catalysis. *Chem. Soc. Rev.* **2004**, *33*, 619–636. [CrossRef] [PubMed]
18. Janssen-Müller, D.; Schlepphorst, C.; Glorius, F. Privileged Chiral N-Heterocyclic Carbene Ligands for Asymmetric Transition-Metal Catalysis. *Chem. Soc. Rev.* **2017**, *46*, 4845–4854. [CrossRef]
19. Foster, D.; Borhanuddin, S.M.; Dorta, R. Designing Successful Monodentate N-Heterocyclic Carbene Ligands for Asymmetric Metal Catalysis. *Dalton Trans.* **2021**, *50*, 17467–17477. [CrossRef]
20. Costabile, C.; Pragliola, S.; Grisi, F. C2-Symmetric N-Heterocyclic Carbenes in Asymmetric Transition-Metal Catalysis. *Symmetry* **2022**, *14*, 1615. [CrossRef]
21. Samojłowicz, C.; Bieniek, M.; Grela, K. Ruthenium-Based Olefin Metathesis Catalysts Bearing *N* -Heterocyclic Carbene Ligands. *Chem. Rev.* **2009**, *109*, 3708–3742. [CrossRef]
22. Vougioukalakis, G.C.; Grubbs, R.H. Ruthenium-Based Heterocyclic Carbene-Coordinated Olefin Metathesis Catalysts. *Chem. Rev.* **2010**, *110*, 1746–1787. [CrossRef]
23. Bieniek, M.; Michrowska, A.; Usanov, D.L.; Grela, K. In an Attempt to Provide a User's Guide to the Galaxy of Benzylidene, Alkoxybenzylidene, and Indenylidene Ruthenium Olefin Metathesis Catalysts. *Chem. Eur. J.* **2008**, *14*, 806–818. [CrossRef]
24. Ogba, O.M.; Warner, N.C.; O'Leary, D.J.; Grubbs, R.H. Recent Advances in Ruthenium-Based Olefin Metathesis. *Chem. Soc. Rev.* **2018**, *47*, 4510–4544. [CrossRef] [PubMed]
25. Paradiso, V.; Costabile, C.; Grisi, F. NHC Backbone Configuration in Ruthenium-Catalyzed Olefin Metathesis. *Molecules* **2016**, *21*, 117. [CrossRef]
26. Paradiso, V.; Costabile, C.; Grisi, F. Ruthenium-Based Olefin Metathesis Catalysts with Monodentate Unsymmetrical NHC Ligands. *Beilstein J. Org. Chem.* **2018**, *14*, 3122–3149. [CrossRef] [PubMed]

27. Montgomery, T.P.; Johns, A.M.; Grubbs, R.H. Recent Advancements in Stereoselective Olefin Metathesis Using Ruthenium Catalysts. *Catalysts* **2017**, *7*, 87. [CrossRef]
28. Hamad, F.B.; Sun, T.; Xiao, S.; Verpoort, F. Olefin Metathesis Ruthenium Catalysts Bearing Unsymmetrical Heterocylic Carbenes. *Coord. Chem. Rev.* **2013**, *257*, 2274–2292. [CrossRef]
29. Tornatzky, J.; Kannenberg, A.; Blechert, S. New Catalysts with Unsymmetrical N-Heterocyclic Carbene Ligands. *Dalton Trans.* **2012**, *41*, 8215. [CrossRef]
30. Monsigny, L.; Kajetanowicz, A.; Grela, K. Ruthenium Complexes Featuring Unsymmetrical N-Heterocyclic Carbene Ligands–Useful Olefin Metathesis Catalysts for Special Tasks. *Chem. Rec.* **2021**, *21*, 3648–3661. [CrossRef]
31. Al Samak, B.; Carvill, A.G.; Rooney, J.J.; Thompson, J.M. Alternating Ring-Opening Metathesis Copolymerization of Bicyclo[2.2.1]Hept-2-Ene and Cyclopentene. *Chem. Commun.* **1997**, *21*, 2057–2058. [CrossRef]
32. Ilker, M.F.; Coughlin, E.B. Alternating Copolymerizations of Polar and Nonpolar Cyclic Olefins by Ring-Opening Metathesis Polymerization. *Macromolecules* **2002**, *35*, 54–58. [CrossRef]
33. Bornand, M.; Chen, P. Mechanism-Based Design of a ROMP Catalyst for Sequence-Selective Copolymerization. *Angew. Chem. Int. Ed.* **2005**, *44*, 7909–7911. [CrossRef]
34. Bornand, M.; Torker, S.; Chen, P. Mechanistically Designed Dual-Site Catalysts for the Alternating ROMP of Norbornene and Cyclooctene. *Organometallics* **2007**, *26*, 3585–3596. [CrossRef]
35. Torker, S.; Müller, A.; Sigrist, R.; Chen, P. Tuning the Steric Properties of a Metathesis Catalyst for Copolymerization of Norbornene and Cyclooctene toward Complete Alternation. *Organometallics* **2010**, *29*, 2735–2751. [CrossRef]
36. Torker, S.; Müller, A.; Chen, P. Building Stereoselectivity into a Chemoselective Ring-Opening Metathesis Polymerization Catalyst for Alternating Copolymerization. *Angew. Chem.* **2010**, *122*, 3850–3854. [CrossRef]
37. Vehlow, K.; Wang, D.; Buchmeiser, M.R.; Blechert, S. Alternating Copolymerizations Using a Grubbs-Type Initiator with an Unsymmetrical, Chiral N-Heterocyclic Carbene Ligand. *Angew. Chem. Int. Ed.* **2008**, *47*, 2615–2618. [CrossRef]
38. Lichtenheldt, M.; Wang, D.; Vehlow, K.; Reinhardt, I.; KÃ¼hnel, C.; Decker, U.; Blechert, S.; Buchmeiser, M. Alternating Ring-Opening Metathesis Copolymerization by Grubbs-Type Initiators with Unsymmetrical N-Heterocyclic Carbenes. *Chem. Eur. J.* **2009**, *15*, 9451–9457. [CrossRef] [PubMed]
39. Buchmeiser, M.R.; Ahmad, I.; Gurram, V.; Kumar, P.S. Pseudo-Halide and Nitrate Derivatives of Grubbs and Grubbs–Hoveyda Initiators: Some Structural Features Related to the Alternating Ring-Opening Metathesis Copolymerization of Norborn-2-Ene with Cyclic Olefins. *Macromolecules* **2011**, *44*, 4098–4106. [CrossRef]
40. Engl, P.S.; Fedorov, A.; Copéret, C.; Togni, A. *N*-Trifluoromethyl NHC Ligands Provide Selective Ruthenium Metathesis Catalysts. *Organometallics* **2016**, *35*, 887–893. [CrossRef]
41. Vasiuta, R.; Stockert, A.; Plenio, H. Alternating Ring-Opening Metathesis Polymerization by Grubbs-Type Catalysts with *N* -Pentiptycenyl, *N* -Alkyl-NHC Ligands. *Chem. Commun.* **2018**, *54*, 1706–1709. [CrossRef] [PubMed]
42. Paradiso, V.; Bertolasi, V.; Grisi, F. Novel Olefin Metathesis Ruthenium Catalysts Bearing Backbone-Substituted Unsymmetrical NHC Ligands. *Organometallics* **2014**, *33*, 5932–5935. [CrossRef]
43. Paradiso, V.; Bertolasi, V.; Costabile, C.; Grisi, F. Ruthenium Olefin Metathesis Catalysts Featuring Unsymmetrical N-Heterocyclic Carbenes. *Dalton Trans.* **2016**, *45*, 561–571. [CrossRef]
44. Paradiso, V.; Grisi, F. Ruthenium-Catalyzed Alternating Ring-Opening Metathesis Copolymerization of Norborn-2-ene with Cyclic Olefins. *Adv. Synth. Catal.* **2019**, *361*, 4133–4139. [CrossRef]
45. Paradiso, V.; Bertolasi, V.; Costabile, C.; Caruso, T.; Dąbrowski, M.; Grela, K.; Grisi, F. Expanding the Family of Hoveyda–Grubbs Catalysts Containing Unsymmetrical NHC Ligands. *Organometallics* **2017**, *36*, 3692–3708. [CrossRef]
46. Sanford, M.S.; Ulman, M.; Grubbs, R.H. New Insights into the Mechanism of Ruthenium-Catalyzed Olefin Metathesis Reactions. *J. Am. Chem. Soc.* **2001**, *123*, 749–750. [CrossRef] [PubMed]
47. Sanford, M.S.; Love, J.A.; Grubbs, R.H. Mechanism and Activity of Ruthenium Olefin Metathesis Catalysts. *J. Am. Chem. Soc.* **2001**, *123*, 6543–6554. [CrossRef] [PubMed]
48. Love, J.A.; Sanford, M.S.; Day, M.W.; Grubbs, R.H. Synthesis, Structure, and Activity of Enhanced Initiators for Olefin Metathesis. *J. Am. Chem. Soc.* **2003**, *125*, 10103–10109. [CrossRef] [PubMed]
49. Vougioukalakis, G.C.; Grubbs, R.H. Ruthenium-Based Olefin Metathesis Catalysts Coordinated with Unsymmetrical N-Heterocyclic Carbene Ligands: Synthesis, Structure, and Catalytic Activity. *Chem. Eur. J.* **2008**, *14*, 7545–7556. [CrossRef] [PubMed]
50. Vorfalt, T.; Wannowius, K.-J.; Plenio, H. Probing the Mechanism of Olefin Metathesis in Grubbs-Hoveyda and Grela Type Complexes. *Angew. Chem. Int. Ed.* **2010**, *49*, 5533–5536. [CrossRef]
51. Thiel, V.; Hendann, M.; Wannowius, K.-J.; Plenio, H. On the Mechanism of the Initiation Reaction in Grubbs–Hoveyda Complexes. *J. Am. Chem. Soc.* **2012**, *134*, 1104–1114. [CrossRef]
52. Nuñez-Zarur, F.; Solans-Monfort, X.; Rodríguez-Santiago, L.; Sodupe, M. Differences in the Activation Processes of Phosphine-Containing and Grubbs–Hoveyda-Type Alkene Metathesis Catalysts. *Organometallics* **2012**, *31*, 4203–4215. [CrossRef]
53. Piers, W.E. Olefin Metathesis and Metathesis Polymerization By K. J. Ivin (The Queen's University of Belfast) and J. C. Mol (University of Amsterdam). Academic Press: San Diego. 1997. Xvi + 472 Pp. $70.00. ISBN 0-12-377045-9. *J. Am. Chem. Soc.* **1997**, *119*, 8396. [CrossRef]

54. Falivene, L.; Credendino, R.; Poater, A.; Petta, A.; Serra, L.; Oliva, R.; Scarano, V.; Cavallo, L. SambVca 2. A Web Tool for Analyzing Catalytic Pockets with Topographic Steric Maps. *Organometallics* **2016**, *35*, 2286–2293. [CrossRef]
55. Falivene, L.; Cao, Z.; Petta, A.; Serra, L.; Poater, A.; Oliva, R.; Scarano, V.; Cavallo, L. Towards the Online Computer-Aided Design of Catalytic Pockets. *Nat. Chem.* **2019**, *11*, 872–879. [CrossRef] [PubMed]
56. Dorta, R.; Stevens, E.D.; Scott, N.M.; Costabile, C.; Cavallo, L.; Hoff, C.D.; Nolan, S.P. Steric and Electronic Properties of N-Heterocyclic Carbenes (NHC): A Detailed Study on Their Interaction with $Ni(CO)_4$. *J. Am. Chem. Soc.* **2005**, *127*, 2485–2495. [CrossRef] [PubMed]
57. Cavallo, L.; Correa, A.; Costabile, C.; Jacobsen, H. Steric and Electronic Effects in the Bonding of N-Heterocyclic Ligands to Transition Metals. *J. Organomet. Chem.* **2005**, *690*, 5407–5413. [CrossRef]
58. Frisch, M.J.; Trucks, G.W.; Schlegel, H.B.; Scuseria, G.E.; Robb, M.A.; Cheeseman, J.R.; Scalmani, G.; Barone, V.; Mennucci, B.; Petersson, G.A.; et al. *Gaussian 09, Revision A.02*; Gaussian, Inc.: Wallingford, CT, USA, 2009.
59. Becke, A. D. Density-functional exchange-energy approximation with correct asymptotic behavior. *Phys. Rev. A* **1988**, *38*, 3098–3100. [CrossRef] [PubMed]
60. Perdew, J. P. Density-functional approximation for the correlation energy of the inhomogeneous electron gas. *Phys. Rev. B* **1986**, *33*, 8822–8824, Erratum in *Phys. Rev. B* **1986**, *34*, 7406–7406. [CrossRef]
61. Schaefer, A.; Horn, H.; Ahlrichs, R. Fully optimized contracted Gaussian basis sets for atoms Li to Kr. *J. Chem. Phys.* **1992**, *97*, 2571–2577. [CrossRef]
62. Haeusermann, U.; Dolg, M.; Stoll, H.; Preuss, H.; Schwerdtfeger, P.; Pitzer, R.M. Accuracy of energy-adjusted quasirelativistic ab initio pseudopotentials. *Mol. Phys.* **1993**, *78*, 1211–1224. [CrossRef]
63. Kuechle, W.; Dolg, M.; Stoll, H.; Preuss, H. Energy—Adjusted pseudopotentials for the actinides. Parameter sets and test calculations for thorium and thorium monoxide. *J. Chem. Phys.* **1994**, *100*, 7535–7542. [CrossRef]
64. Leininger, T.; Nicklass, A.; Stoll, H.; Dolg, M.; Schwerdtfeger, P. The accuracy of the pseudopotential approximation. II. A comparison of various core sizes for indium pseudopotentials in calculations for spectroscopic constants of InH, InF, and InCl. *J. Chem. Phys.* **1996**, *105*, 1052–1059. [CrossRef]
65. Clark, T.; Chandrasekhar, J.; Spitznagel, G.W.; Schleyer, P.v.R. Efficient diffuse function-augmented basis-sets for anion calculations. 3. The 3-21+G basis set for 1st-row elements, Li-F. *J. Comp. Chem.* **1983**, *4*, 294–301. [CrossRef]
66. Barone, V.; Cossi, M. Quantum Calculation of Molecular Energies and Energy Gradients in Solution by a Conductor Solvent Model. *J. Phys. Chem. A* **1998**, *102*, 1995–2001. [CrossRef]
67. Tomasi, J.; Persico, M. Molecular Interactions in Solution: An Overview of Methods Based on Continuous Distributions of the Solvent. *Chem. Rev.* **1994**, *94*, 2027–2094. [CrossRef]